Soil Dynamics and Earthquake Engineering 196 (2025) 109511

Contents lists available at ScienceDirect

Soil Dynamics and Earthquake Engineering

journal homepage: www.elsevier.com/locate/soildyn

Vibration of inclined piles in transversely isotropic soils

Hamed Moghaddasi [a], Babak Shahbodagh [b,*], Ali Khojasteh [c], Mohammad Rahimian [d]

[a] Department of Civil and Environmental Engineering, University of Strathclyde, Glasgow, G1 1XQ, Scotland, UK
[b] School of Civil and Environmental Engineering, University of New South Wales, Sydney, 2052, Australia
[c] School of Engineering Science, University of Tehran, Tehran, Iran
[d] School of Civil Engineering, University of Tehran, Tehran, Iran

ARTICLE INFO

Keywords:
Inclined piles
Soil anisotropy
Dynamic soil-pile interaction
Interaction factor
Hybrid analytical-numerical method

ABSTRACT

This paper studies the dynamic behavior of inclined piles in transversely isotropic soils using a hybrid analytical-numerical approach. Inclined piles subjected to various vibration modes are modeled using the three-dimensional dynamic Bernoulli-Euler beam theory. The dynamic interaction between the inclined piles and the surrounding transversely isotropic soil is represented by a series of rigid radiation discs defined at the nodal points of the beam elements. The Green's functions governing the dynamic response of the radiation discs embedded in the transversely isotropic medium are derived using complete potential functions. The Green's functions fully satisfy the regularity conditions at infinity, eliminating the spurious wave reflections within the domain, addressing a major challenge in most numerical methods for dynamic soil-pile interactions. The dynamic impedance functions for inclined piles are determined, and the coupled influence of various parameters, including pile inclination angle, soil anisotropy, and excitation frequency on the dynamic pile-soil interaction is highlighted. The dynamic interaction factors for inclined piles embedded in transversely isotropic soils are also presented, essential for the design and analysis of pile groups subjected to vibrations.

1. Introduction

Inclined piles, often referred to as batter piles, play a key role in the stability of structures exposed to dynamic loads, including lateral forces induced by earthquakes, winds, and water waves. A key advantage of these foundations, compared to vertical piles, is their ability to mobilise both axial and transverse stiffness during lateral vibrations, thus exhibiting greater horizontal stiffness compared to vertical piles of the same dimensions. Numerous research works have studied the response of inclined piles subjected to various modes of vibration (e.g., see Refs. [1–10]). These studies, however, mostly assumed isotropic behavior for the surrounding soil to reduce the complexity of numerical and analytical analysis. Real soils, however, inherently exhibit anisotropic characteristics due to their natural depositional processes, which can notably affect the dynamic strength and stiffness of the piles and pile groups. The anisotropy leads to varying resistance across different directions in the soil medium, potentially influencing the performance of structures under specific loading conditions.

In the context of dynamic pile-soil interaction analysis, Pak and Jennings [11] and Pak [12] presented rigorous analytical solutions for the lateral movement of vertical piles in an isotropic elastic half-space using the Fredholm integral equation. In this approach, the displacement compatibility between the pile and soil was enforced along the entire length of the pile. Despite the rigour of their mathematical formulation, it would be cumbersome to extend this approach for inclined piles, especially when they are placed in pile groups. For these complex cases, directly enforcing displacement compatibility along the entire pile-soil interface would lead to coupled mixed boundary value problems, necessitating computationally intensive numerical solutions. Rajapakse and Shah [13] investigated lateral and vertical vibrations of vertical piles in an isotropic half-space using Green's functions for dynamic cases. More recently, Liu et al. [14] analytically studied the vertical vibration of a pipe pile in an isotropic half-space for a single-layer soil, while Ai and Liu [15] extended this study to multi-layered soils. For complex pile geometries, Mamoon et al. [2] implemented 3D Green's functions within the boundary element method (BEM) to determine the dynamic stiffness of inclined pile groups. Makris and Gazetas [16] proposed a semi-analytical beam-on-Winkler foundation approach to analyze inclined beam vibrations. This approach was later incorporated by Ghasemzadeh and Alibeikloo [7] for the dynamic analysis of inclined piles using the Euler-beam theory, and by Wang et al. [8] for the dynamic analysis of piles with low slenderness ratios using the Timoshenko

* Corresponding author.
E-mail address: b.shahbodagh@unsw.edu.au (B. Shahbodagh).

https://doi.org/10.1016/j.soildyn.2025.109511
Received 18 December 2024; Received in revised form 5 May 2025; Accepted 8 May 2025

beam theory. However, since independent elements, i.e., springs and dashpots, were used to represent the soil, the method cannot comprehensively capture the three-dimensional dynamic behavior of the soil and the interactions between adjacent piles. To overcome this challenge, Giannakou et al. [3] employed the finite element method (FEM) for the analysis of inclined piles under vibrations. Pardon et al. [5], Medina et al. [17], and Medina et al. [18] adopted a coupled Boundary Element Method-Finite Element Method (BEM-FEM) approach for the dynamic analysis of both floating and end-bearing inclined pile groups. Most numerical approaches, however, present computational challenges due to the necessity of enforcing radiation conditions for the soil medium. These regularity conditions are essential for eliminating spurious wave reflections in dynamic pile-soil interaction problems and accurately simulating the unbounded domain surrounding the piles.

Recognizing the importance of soil anisotropy, many researchers have adopted transverse isotropy as a common assumption for describing anisotropy in geological formations. This approach effectively accounts for the natural deposition of soil layers and the depth-wise effects of gravity in the constitutive equations. Wang and Rajapakse [19] formulated the lateral and vertical vibrations of a vertical pile in a transversely isotropic medium using ring-load Green's functions, while Barros [20] employed the indirect Boundary Element Method (BEM) for this analysis. Using the integral equation approach developed by Pak and Jennings [11], Shahmohamadi et al. [21] rigorously examined the vertical vibration of a thin-walled vertical pile, and Gharahi et al. [22] investigated the lateral vibration of a vertical bar in a transversely isotropic half-space. Amiri-Hezaveh et al. [23] studied the dynamic behavior of a buried foundation in a non-homogeneous transversely isotropic half-space using the fundamental solutions developed by Eskandari-Ghadi and Amiri-Hezaveh [24] for functionally graded anisotropic materials. Karimi et al. [25] investigated the dynamic behavior of a multi-layered transversely isotropic half-space subjected to the excitation of a surface foundation. Ai and Cao [26] and Zhang et al. [27] investigated the dynamic response of pile groups in multi-layered dry and saturated transversely isotropic soils. Ai et al. [28] investigated the dynamic behavior of partially embedded vertical piles in transversely isotropic soils. Despite the precise mathematical formulations, an analytical approach is challenging to employ for complex pile-soil configurations, including inclined piles and pile groups. Shahbodagh et al. [29] presented an analytical-numerical hybrid element method for the vibration analysis of piles and pile groups in a transversely isotropic half-space. The approach was later generalized by Moghaddasi et al. [30] to the lateral vibration of piles and pile groups in a non-homogeneous transversely isotropic half-space. This approach can analytically capture the 3D non-homogeneity of anisotropic half-space without incorporating simplifying assumptions, such as dividing the soil into a series of homogeneous zones.

In the context of pile groups, interaction factors are routinely employed in geotechnical engineering practice to capture the influence of pile-soil-pile interaction. Early work by Poulos [31] demonstrated how the superposition of the two-pile interaction effect could be used to estimate the displacement of a pile group, facilitating an approach commonly referred to as the superposition method. While static interaction factors are sufficient for low-frequency scenarios, they are generally inadequate for higher-frequency or transient loading conditions. Kaynia [32] and Mamoon et al. [5] validated that Poulos' superposition method can provide an excellent engineering solution if dynamically derived interaction factors, reflecting frequency-dependent soil-pile behavior, are employed in the design and analysis of pile groups. Motivated by these insights, further studies focused on deriving dynamic interaction factors under varying conditions. Kaynia [32] and Gazetas et al. [33] used a rigorous superposition-based approach to calculate dynamic interaction factors for vertically floating piles, while Dobry and Gazetas [34] adopted an approximate analytical solution anchored in cylindrical wave expressions. Mylonakis and Gazetas [35] further extended these principles to derive interaction factors for laterally vibrating piles in multi-layered soils using a dynamic Winkler model. More recent investigations by Ghasemzadeh and Alibeikloo [7] and Wang et al. [8] adapted these frameworks to compute interaction factors for inclined piles in isotropic soils. The previous studies, however, largely neglected the combined effects of soil anisotropy, pile inclination angle, load frequency, and partial embedment, all of which can significantly influence the dynamic response of pile groups.

In light of these gaps, this paper presents a generalized framework for the analysis of inclined piles in transversely isotropic soils subjected to different vibration modes. This research expands the numerical-analytical model of Shahbodagh et al. [29] by incorporating the coupled effects of pile inclination angle, partial embedment, load frequency, and soil anisotropy. The inclined piles are modeled using the three-dimensional dynamic Bernoulli-Euler beam theory. To account for the pile's inclination angle, the model incorporates both axial and transverse vibrations, allowing for modeling the dynamic behavior of piles subjected to various loading conditions. A series of rigid radiation discs are introduced at the nodes of the pile elements to simulate the dynamic interactions of the inclined piles in the semi-infinite transversely isotropic medium. The study leverages complete displacement potential functions (see Eskandari-Ghadi [36], Khojasteh et al. [37]) for transversely isotropic materials in conjunction with the integral transform method to determine the complete solutions for radiation discs subjected to various modes of excitations. A Boussinesq-type loading pattern is considered on the radiation discs to achieve the realistic mode of deformation along the pile cross-sections [29,30,38]. The Green's functions fully satisfy the regularity conditions at infinity, eliminating the spurious wave reflections within the domain. The model is validated using the existing analytical and numerical solutions for an inclined pile in an isotropic half-space. The effects of soil anisotropy, pile inclination angle, and excitation frequency on the dynamic impedance functions of an inclined pile embedded in a transversely isotropic half-space is explored and discussed. Unlike most existing models focusing on vibrating vertical piles, the proposed approach focuses on inclined piles with full or partial embedment in soils subjected to various modes of vibrations. The model captures the coupled interactions between pile inclination angle and degree of soil anisotropy, an aspect that has not been rigorously covered in the previous studies. The solutions obtained in this study can be used as benchmark examples for the verification of numerical simulations addressing dynamic soil-pile interaction problems in the fields of geotechnical and offshore engineering.

2. Hybrid element method for dynamic interaction of inclined pile-soil system

An inclined cylindrical pile placed in a transversely isotropic half-space is considered in this study. The pile has an inclination angle β aligned with the vertical axis and is subjected to various modes of vibrations at its head. The pile and surrounding medium are occupied the regions Ω_p and Ω_s, respectively, and are in contact with each other at the interface Γ (see Fig. 1). The fully bonded contact is assumed between the pile and surrounding materials.

Due to the linearity of the elasto-dynamic pile-soil system, the superposition principle is applied, allowing the inclined pile-soil system to be divided into two separate systems. An extended soil medium (Fig. 2a) is created by assuming that the pile region Ω_p is filled by the same material of soils. The fictitious pile system is then introduced such that the superposition of the two systems replicates the behavior of the actual pile-soil system (Fig. 2b). The interaction of the pile-soil system under dynamic cases is addressed by applying displacement/traction compatibility conditions along the pile region Ω_p in both systems.

Within the extended soil medium, the governing equations in the Cartesian framework can be expressed as:

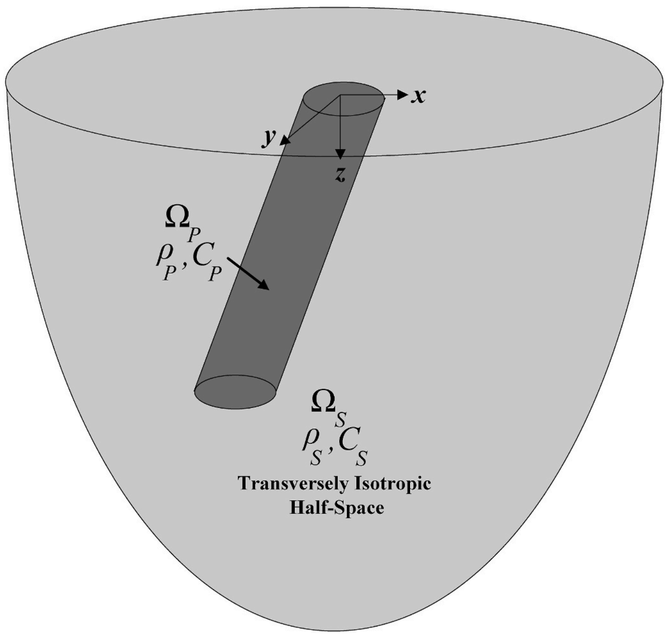

Fig. 1. The inclined pile embedded in a semi-infinite soil with transversely isotropic behavior.

$$\begin{cases} \sigma_{Sji,j} + f_{Si} = \rho_S \ddot{u}_{Si} \quad \text{on } \Omega_S \\ \sigma^e_{Pji,j} + f^e_{Pi} = \rho_S \ddot{u}_{Pi} \quad \text{on } \Omega_P \end{cases} \tag{1}$$

$$\begin{cases} \sigma_{Sij} = \dfrac{C_{Sijkl}}{2}(u_{Sk,l} + u_{Sl,k}) \quad \text{on } \Omega_S \\ \sigma^e_{Pij} = \dfrac{C_{Sijkl}}{2}(u_{Pk,l} + u_{Pl,k}) \quad \text{on } \Omega_P \end{cases} \tag{2}$$

$$u_{Si} = u_{Pi}, \left(\sigma^e_{Pij} - \sigma_{Sij}\right) n_j = T^e_i \quad \text{on } \Gamma \tag{3}$$

where $u_{\alpha i}(\alpha = S, P)$ are the displacement components, $\sigma_{\alpha ij}$ is the Cauchy stress tensor, $f_{\alpha i}$ stands for the vector of body force, and T_i denotes the traction vector on Γ. The subscripts S and P indicate the respective quantities associated with the area occupied with soil medium and the pile region, and the superscript e indicates the corresponding quantities of the region within the extended soil medium. For the fictitious pile system, the governing equations become

$$\sigma^f_{Sij} = 0, f^f_{Si} = 0 \quad \text{on } \Omega_S \tag{4}$$

$$\sigma^f_{Pji,j} + f^f_{Pi} = (\rho_p - \rho_S) \ddot{u}_{Pi} \quad \text{on } \Omega_P \tag{5}$$

$$\sigma^f_{Pij} = \frac{(C_{Pijkl} - C_{Sijkl})}{2}(u_{Pk,l} + u_{Pk,l}) \quad \text{on } \Omega_P \tag{6}$$

$$\sigma^f_{Pji} n_j = T^f_i \quad \text{on } \Gamma \tag{7}$$

where the superscript f stands for the corresponding quantities of the fictitious pile system. Combining the equations for two systems, it can be seen that $\sigma^e_{Pij} + \sigma^f_{Pij} = \sigma_{Pij}, f^e_{Pi} + f^f_{Pi} = f_{Pi}, T^e_i + T^f_i = T_i$. The arrangements for the body forces ($f^e_{P\,i}$ and $f^f_{P\,i}$) and the tractions on decomposed systems (T^e_i and T^f_i) are defined in a manner that ensures they produce the identical field variables (e.g. displacements) in both systems. In practical applications, piles frequently exhibit high slenderness ratio ($l/a \gg 1$) and high pile-soil stiffness ratio ($C_{Pijkl}/C_{Sijkl} \gg 1$). Hence, the Bernoulli-Euler beam-column theory is selected for the inclined fictitious pile and solved using FEM (see Fig. 3a). The equations of motion for an inclined pile element in the local coordinate system is written as (see Appendix A)

$$E_e I_P \frac{\partial^4 \overline{y}(\overline{z}, t)}{\partial \overline{z}^4} + \rho_e A_P \frac{\partial^2 \overline{y}(\overline{z}, t)}{\partial t^2} = 0 \tag{8}$$

$$E_e \frac{\partial^2 \overline{w}(\overline{z}, t)}{\partial \overline{z}^2} - \rho_e \frac{\partial^2 \overline{w}(\overline{z}, t)}{\partial t^2} = 0 \tag{9}$$

where $\rho_e = \rho_P - \rho_S$, $E_e = E_P - E_S$, ρ_S and ρ_P are the density, and E_S and E_P are the elastic moduli of the soil and pile, respectively. $\overline{y}(\overline{z}, t)$ and $\overline{w}(\overline{z}, t)$ are the lateral and vertical displacements of the pile along the longitudinal axis of the pile, respectively, $E_e I_p$ is the flexural rigidity of the element, and A_P is the profile area of the pile perpendicular to $\overline{z}$. The analytical approach to find the solution of the system of equations (8) and (9) is presented in appendix A. In the global reference frame, the dynamic stiffness matrix of an inclined pile with N-1 elements are denoted by $[K_P]_{3N \times 3N}$.

To evaluate the dynamic stiffness matrix of the extended soil domain, a number of radiation discs subjected to vibrations are introduced at the nodes of the beam-column elements (see Fig. 3b). Assuming N radiation discs over the length of the inclined pile, consistent with the number of nodes defined on the fictitious pile, the flexibility matrix of the extended soil domain in dynamic, $[C_S]$, can be obtained. Each row of the flexibility matrix can be calculated by exciting the soil at the radiation disc i and

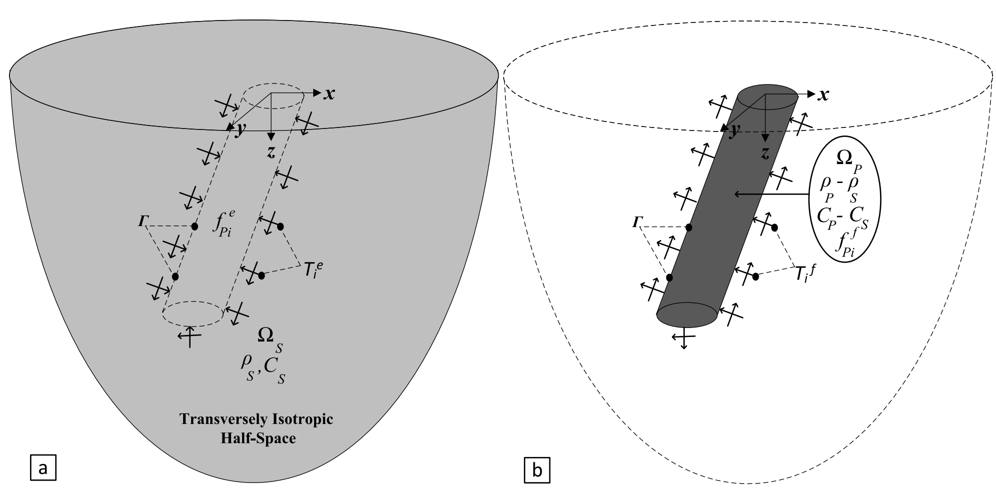

Fig. 2. Decomposing the inclined pile-soil system into a) an extended half-space, and b) a fictitious inclined pile.

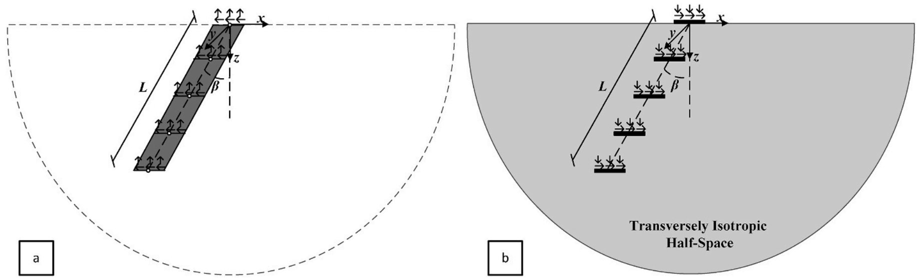

Fig. 3. The hybrid element method: a) discretization of the inclined pile, b) radiation discs representing the dynamic pile-soil interaction.

determining the corresponding displacements at the other radiation discs. Finally, by inverting the flexibility matrix $[C_S]_{3N\times 3N}$, the dynamic stiffness matrix of the extended soil system $[K_S]_{3N\times 3N}$ is obtained. The total dynamic stiffness matrix of the pile-soil system can be determined as $[K_T] = [K_P] + [K_S]$. The relation between forces and displacements for the inclined pile-soil system can be written as

$$\left\{\begin{array}{c}\{F\}\\ \{V\}\\ \{M\}\end{array}\right\}_{3N\times 1} = \begin{bmatrix}[K_{zz}] & [K_{zy}] & [K_{z\theta}]\\ [K_{yz}] & [K_{yy}] & [K_{y\theta}]\\ [K_{\theta z}] & [K_{\theta y}] & [K_{\theta\theta}]\end{bmatrix}_{3N\times 3N} \left\{\begin{array}{c}\{W\}\\ \{Y\}\\ \{\Theta\}\end{array}\right\}_{3N\times 1} \tag{10}$$

in which $\{Y\}$ and $\{V\}$ are the vectors pertaining to the lateral displacements and forces, $\{W\}$ and $\{F\}$ are the vertical deformations and vertical forces vectors, and $\{\Theta\}$ and $\{M\}$ are the vectors of rotation angles and bending moments, respectively.

3. Governing equations for transversely isotropic half-space

The extended soil medium is defined as a transversely isotropic elastic half-space, in which the axis of symmetry of the medium aligns with the normal to the horizontal surface. A cylindrical coordinate system is considered on the horizontal surface. The constitutive equation for the transversely isotopic medium in the cylindrical coordinate system is expressed as

$$\begin{bmatrix}\sigma_{rr}\\ \sigma_{\theta\theta}\\ \sigma_{zz}\\ \sigma_{rz}\\ \sigma_{\theta z}\\ \sigma_{r\theta}\end{bmatrix} = \begin{bmatrix} c_{11} & c_{12} & c_{13} & 0 & 0 & 0\\ c_{12} & c_{11} & c_{13} & 0 & 0 & 0\\ c_{13} & c_{13} & c_{33} & 0 & 0 & 0\\ 0 & 0 & 0 & 2c_{44} & 0 & 0\\ 0 & 0 & 0 & 0 & 2c_{44} & 0\\ 0 & 0 & 0 & 0 & 0 & 2c_{66}\end{bmatrix} \begin{bmatrix}\varepsilon_{rr}\\ \varepsilon_{\theta\theta}\\ \varepsilon_{zz}\\ \varepsilon_{rz}\\ \varepsilon_{\theta z}\\ \varepsilon_{r\theta}\end{bmatrix} \tag{11}$$

in which σ_{ij} $(i,j = r,\theta,z)$ and ε_{ij} $(i,j = r,\theta,z)$ are the stress and strain tensors. The material constants of the medium, c_{ij}, are expressed as

$$c_{11} = \frac{E_S\left(1-\frac{E_S}{E'_S}\nu'^{\,2}_S\right)}{(1+\nu_S)\left(1-\nu_S-2\frac{E_S}{E'_S}\nu'^{\,2}_S\right)}, c_{13} = \frac{E_S\nu'_S}{\left(1-\nu_S-2\frac{E_S}{E'_S}\nu'^{\,2}_S\right)}, c_{44} = G'_S$$
$$c_{33} = \frac{E'_S(1-\nu_S)}{\left(1-\nu_S-2\frac{E_S}{E'_S}\nu'^{\,2}_S\right)}, c_{66} = \frac{E_S}{2(1+\nu_S)} = G_S, c_{12} = c_{11}-2c_{66} \tag{12}$$

where E_S and E'_S are the Young's moduli parallel to and perpendicular to the plane of isotropy, ν_S and ν'_S are the Poisson's ratios for in-plane and normal directions, and G_S and G'_S are the shear moduli along and perpendicular to the isotropic plane, respectively. When body forces are neglected, the equations of motion for the transversely isotropic medium subjected to time-harmonic vibrations can be expressed as

$$\begin{aligned}
&\frac{\partial\sigma_{rr}}{\partial r}+\frac{1}{r}\frac{\partial\sigma_{\theta r}}{\partial\theta}+\frac{1}{r}(\sigma_{rr}-\sigma_{\theta\theta})+\frac{\partial\sigma_{zr}}{\partial z}+\rho_s\omega^2u_r=0,\\
&\frac{\partial\sigma_{r\theta}}{\partial r}+\frac{1}{r}\frac{\partial\sigma_{\theta\theta}}{\partial\theta}+\frac{2}{r}\sigma_{r\theta}+\frac{\partial\sigma_{z\theta}}{\partial z}+\rho_s\omega^2u_\theta=0\\
&\frac{\partial\sigma_{rz}}{\partial r}+\frac{1}{r}\frac{\partial\sigma_{\theta z}}{\partial\theta}+\frac{1}{r}\sigma_{rz}+\frac{\partial\sigma_{zz}}{\partial z}+\rho_s\omega^2u_z=0.
\end{aligned} \tag{13}$$

in which ρ_s is the soil density, $u_i(i,j=r,\theta,z)$ is the displacement vector (i.e. the vibration amplitude vector), and ω is the circular frequency of the excitation. The time factor $e^{i\omega t}$ is omitted in the equations. Utilizing the stress-strain relation (11), the equations of motion in terms of the vibration amplitudes can be obtained as

$$\begin{aligned}
&c_{11}\left(\frac{\partial^2u_r}{\partial r^2}+\frac{1}{r}\frac{\partial u_r}{\partial r}-\frac{u_r}{r^2}\right)+c_{66}\frac{1}{r^2}\frac{\partial^2u_r}{\partial\theta^2}+c_{44}\frac{\partial^2u_r}{\partial z^2}+\frac{c_{11}+c_{12}}{2}\left(\frac{1}{r}\frac{\partial^2u_\theta}{\partial r\partial\theta}+\frac{1}{r^2}\frac{\partial u_\theta}{\partial\theta}\right)\\
&\quad-2c_{11}\frac{1}{r^2}\frac{\partial u_\theta}{\partial\theta}+(c_{13}+c_{44})\frac{\partial^2u_z}{\partial r\partial z}+\rho_s\omega^2u_r=0,\\
&c_{66}\left(\frac{\partial^2u_\theta}{\partial r^2}+\frac{1}{r}\frac{\partial u_\theta}{\partial r}-\frac{u_\theta}{r^2}\right)+c_{11}\frac{1}{r^2}\frac{\partial^2u_\theta}{\partial\theta^2}+c_{44}\frac{\partial^2u_\theta}{\partial z^2}+\frac{c_{11}+c_{12}}{2}\left(\frac{1}{r}\frac{\partial^2u_r}{\partial r\partial\theta}-\frac{1}{r^2}\frac{\partial u_r}{\partial\theta}\right)\\
&\quad+2c_{11}\frac{1}{r^2}\frac{\partial u_r}{\partial\theta}+(c_{13}+c_{44})\frac{1}{r}\frac{\partial^2u_z}{\partial\theta\partial z}+\rho_s\omega^2u_\theta=0,\\
&c_{44}\left(\frac{\partial^2u_z}{\partial r^2}+\frac{1}{r}\frac{\partial u_z}{\partial r}+\frac{1}{r^2}\frac{\partial^2u_z}{\partial\theta^2}\right)+c_{33}\frac{\partial^2u_z}{\partial z^2}+(c_{13}+c_{44})\left(\frac{\partial^2u_r}{\partial r\partial z}+\frac{1}{r}\frac{\partial u_r}{\partial z}+\frac{1}{r}\frac{\partial^2u_\theta}{\partial\theta\partial z}\right)\\
&\quad+\rho_s\omega^2u_z=0
\end{aligned} \tag{14}$$

These coupled governing equations will be solved utilizing displacement potential functions obtained by Eskandari-Ghadi [36],

$$\begin{aligned}
u_r(r,\theta,z) &= -\alpha_3\frac{\partial^2F(r,\theta,z)}{\partial r\partial z}-\frac{1}{r}\frac{\partial\chi(r,\theta,z)}{\partial\theta},\\
u_\theta(r,\theta,z) &= -\alpha_3\frac{1}{r}\frac{\partial^2F(r,\theta,z)}{\partial\theta\partial z}+\frac{\partial\chi(r,\theta,z)}{\partial r},\\
u_z(r,\theta,z) &= \left[(1+\alpha_1)\nabla^2_{r\theta}+\alpha_2\frac{\partial^2}{\partial z^2}+\frac{\rho_s\omega^2}{c_{66}}\right]F(r,\theta,z).
\end{aligned} \tag{15}$$

where

$$\begin{aligned}
&\nabla^2_{r\theta}=\frac{\partial^2}{\partial r^2}+\frac{1}{r}\frac{\partial}{\partial r}+\frac{1}{r^2}\frac{\partial^2}{\partial\theta^2},\\
&\alpha_1=\frac{c_{12}+c_{66}}{c_{66}}, \alpha_2=\frac{c_{44}}{c_{66}}, \alpha_3=\frac{c_{13}+c_{44}}{c_{66}}
\end{aligned} \tag{16}$$

The functions F and χ act as displacement potential functions, decoupling the governing equations and transforming them into ordinary differential equations (ODEs). This also reduces the number of dependent variables. Physically, F function is associated with the propagation of body waves, while χ function describes the propagation of transverse waves. By substituting Equation (15) into (14), the following two uncoupled equations of motion are derived,

$$\left(\nabla_1^2\nabla_2^2+\delta\omega^2\frac{\partial^2}{\partial z^2}\right)F=0,$$
$$\nabla_0^2\chi=0, \tag{17}$$

where

$$\nabla_i^2=\nabla_{r\theta}^2+\frac{1}{s_i^2}\frac{\partial^2}{\partial z^2}+\frac{1}{\mu_i}\frac{\rho_s\omega^2}{c_{66}}, i=0,1,2$$
$$\mu_0=1,\mu_1=\alpha_2=\frac{c_{44}}{c_{66}},\mu_2=1+\alpha_1=\frac{c_{11}}{c_{66}}, \tag{18}$$
$$\frac{\delta}{\rho_s}=\left[\frac{-1}{c_{44}s_2^2}-\frac{1}{c_{11}s_1^2}+\frac{1}{c_{11}}\left(1+\frac{c_{33}}{c_{44}}\right)\right].$$

In the above equations, s_1^2 and s_2^2 are the roots of

$$c_{33}c_{44}s^4+\left(c_{13}^2+2c_{13}c_{44}-c_{11}c_{33}\right)s^2+c_{11}c_{44}=0 \tag{19}$$

and $s_0=1/\sqrt{\alpha_2}$. Based on the characteristics of the governing equations (17) and the boundary conditions of the problem, a Fourier series expansion with respect to the angular direction $\theta$and the m^{th}-order Hankel transform in the radial direction are introduced

$$\{F(r,\theta,z),\chi(r,\theta,z)\}=\sum_{m=-\infty}^{m=+\infty}\{F_m(r,z),\chi_m(r,z)\}e^{im\theta} \tag{20}$$

$$\{F_m^m(\xi,z),\chi_m^m(\xi,z)\}=\int_0^\infty\{F_m(r,z),\chi_m(r,z)\}rJ_m(\xi r)dr \tag{21}$$

where F_m and χ_m are the m^{th} Fourier coefficient of F and χ, respectively, and J_m is the first kind Bessel function of order m. The application of these transformations to (17) results in

$$\left(\widetilde{\nabla}_{1m}^2\widetilde{\nabla}_{2m}^2+\delta\omega^2\frac{d^2}{dz^2}\right)\widetilde{F}_m^m(\xi,z)=0, \tag{22}$$

$$\widetilde{\nabla}_{0m}^2\widetilde{\chi}_m^m(\xi,z)=0, \tag{23}$$

where

$$\widetilde{\nabla}_{im}^2=\frac{1}{\mu_i}\frac{\rho\omega^2}{c_{66}}-\xi^2+\frac{1}{s_i^2}\frac{d^2}{dz^2}, i=0,1,2 \tag{24}$$

The general solutions of the differential equations (22) and (23) can be expressed as

$$\widetilde{F}_m^m(\xi,z)=A_m(\xi)e^{\lambda_1 z}+B_m(\xi)e^{-\lambda_1 z}+C_m(\xi)e^{\lambda_2 z}+D_m(\xi)e^{-\lambda_2 z}, \tag{25}$$

$$\widetilde{\chi}_m^m(\xi,z)=E_m(\xi)e^{\lambda_3 z}+F_m(\xi)e^{-\lambda_3 z} \tag{26}$$

where

$$\lambda_1=\sqrt{a\xi^2+b+\frac{1}{2}\sqrt{c\xi^4+d\xi^2+e}},$$
$$\lambda_2=\sqrt{a\xi^2+b-\frac{1}{2}\sqrt{c\xi^4+d\xi^2+e}},$$
$$\lambda_3=s_0\sqrt{\xi^2-\frac{\rho_s\omega^2}{c_{66}}}, \tag{27}$$

and

$$a=\frac{1}{2}\left(s_1^2+s_2^2\right),b=-\frac{1}{2}\rho_s\omega^2\left(\frac{1}{c_{33}}+\frac{1}{c_{44}}\right),c=\left(s_2^2-s_1^2\right)^2$$
$$d=-2\rho_s\omega^2\left[\left(\frac{1}{c_{33}}+\frac{1}{c_{44}}\right)\left(s_1^2+s_2^2\right)-2\frac{c_{11}}{c_{33}}\left(\frac{1}{c_{11}}+\frac{1}{c_{44}}\right)\right],e={\rho_s}^2\omega^4\left(\frac{1}{c_{33}}-\frac{1}{c_{44}}\right)^2 \tag{28}$$

The unknowns $A_m(\xi)$ to $H_m(\xi)$ can be obtained by enforcing the set of boundary conditions specified for the problem.

4. Analytical solutions for the radiation discs under vertical and lateral loadings

In this section, the vertical and lateral vibrations of a rigid radiation disc embedded in a transversely isotropic semi-infinite medium are studied. A radiation disc with radius a is considered to be embedded at a depth $z=h$ beneath the ground surface. The area above the disc (where $0\le z<h$) is labelled as Region I, while the half-space below the disc (where $z\ge h$) is labelled as Region II (refer to Fig. 4).

As the lateral movement of an inclined pile can induce both normal and lateral tractions at the pile cross-section, it is essential to develop a solution for circular patch loading encompassing both normal and shear components. The continuity conditions at depth $z=h$, the traction-free condition at the ground surface, and the imposition of traction stress at depth $z=h$ are, respectively, expressed as

$$u_i(r,\theta,z=h^-)=u_i(r,\theta,z=h^+), i=r,\theta,z$$
$$\sigma_{zi}(r,\theta,z=0)=0, i=r,\theta,z$$
$$\sigma_{zz}(r,\theta,z=h^-)-\sigma_{zz}(r,\theta,z=h^+)=R(r,\theta),$$
$$\sigma_{zr}(r,\theta,z=h^-)-\sigma_{zr}(r,\theta,z=h^+)=P(r,\theta)$$
$$\sigma_{z\theta}(r,\theta,z=h^-)-\sigma_{z\theta}(r,\theta,z=h^+)=Q(r,\theta) \tag{29}$$

where $P(r,\theta)$, $Q(r,\theta)$ and $R(r,\theta)$ are radial, tangential and vertical parts of the traction acting on the disc, respectively. The regularity condition for the half-space region requires that the solutions approach zero at infinity, i.e. $C_m^{II}(\xi)=D_m^{II}(\xi)=F_m^{II}(\xi)=0$. Utilizing these conditions, the general solutions of (25) and (26) are obtained as

$$\widetilde{F}_m^m(\xi,z)=A_m^I(\xi)e^{-\lambda_1 z}+B_m^I(\xi)e^{-\lambda_2 z}+C_m^I(\xi)e^{\lambda_1 z}+D_m^I(\xi)e^{\lambda_2 z}, \tag{30}$$

$$\widetilde{\chi}_m^m(\xi,z)=E_m^I(\xi)e^{-\lambda_3 z}+F_m^I(\xi)e^{\lambda_3 z} \tag{31}$$

$$\widetilde{F}_m^m(\xi,z)=A_m^{II}(\xi)e^{-\lambda_1 z}+B_m^{II}(\xi)e^{-\lambda_2 z}, \tag{32}$$

$$\widetilde{\chi}_m^m(\xi,z)=E_m^{II}(\xi)e^{-\lambda_3 z} \tag{33}$$

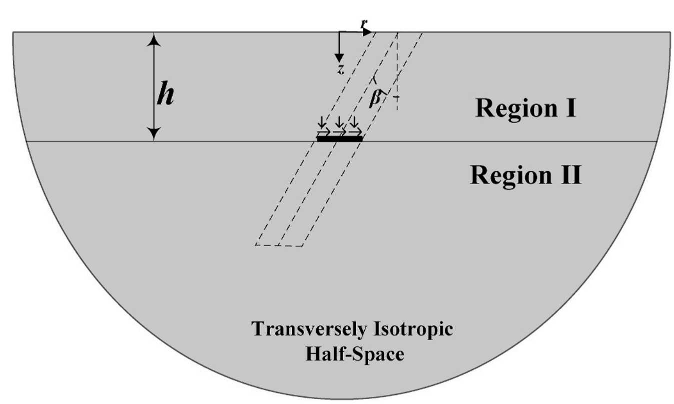

Fig. 4. A radiation disc embedded in a transversely isotropic half-space, subjected to lateral and vertical vibrations.

The displacement solutions for the medium under harmonic excitations are obtained by substituting Equations (30)–(33) into (15), along with the boundary conditions (29),

$$u_{r_m} \mp i u_{\theta_m} = \int_0^\infty \xi \left\{ \pm \gamma_1(\xi,z;h)\frac{X_m - Y_m}{2c_{44}} + \gamma_2(\xi,z;h)\frac{X_m + Y_m}{2c_{44}} \pm \gamma_3(\xi,z;h)\frac{Z_m}{c_{44}} \right\} J_{m\mp1}(r\xi)d\xi \tag{34}$$

$$u_{z_m} = \int_0^\infty \xi \left\{ \Omega_1(\xi,z;h)\frac{X_m(\xi) - Y_m(\xi)}{2c_{44}} + \Omega_2(\xi,z;h)\frac{Z_m(\xi)}{c_{44}} \right\} J_m(r\xi)d\xi \tag{35}$$

where $X_m = P_m^{m-1}(\xi) - iQ_m^{m-1}(\xi)$, $Y_m = P_m^{m+1}(\xi) + iQ_m^{m+1}(\xi)$, $Z_m = R_m^m(\xi)$, and

$$\Omega_1(\xi,z;h) = \frac{\vartheta_1\vartheta_2}{2\alpha_3 c_{33}\left(\eta_1\lambda_2^2 - \eta_2\lambda_1^2\right)} \begin{Bmatrix} \mathrm{sgn}(z-h)\left(e^{-\lambda_1|z-h|} + e^{-\lambda_2|z-h|}\right) - \dfrac{I^+(\xi)}{I^-(\xi)}\left[e^{-\lambda_1|z+h|} + e^{-\lambda_2|z+h|}\right] \\ + \dfrac{2}{I^-(\xi)}\left[\eta_2\nu_2\dfrac{\vartheta_1}{\vartheta_2}e^{-(\lambda_1 z + \lambda_2 h)} + \eta_1\nu_1\dfrac{\vartheta_2}{\vartheta_1}e^{-(\lambda_2 z + \lambda_1 h)}\right] \end{Bmatrix} \tag{36}$$

$$\Omega_2(\xi,z;h) = \frac{c_{44}}{2\alpha_2 c_{33}\left(\lambda_1^2 - \lambda_2^2\right)} \begin{Bmatrix} \dfrac{\vartheta_1}{\lambda_1}e^{-\lambda_1|z-h|} - \dfrac{\vartheta_2}{\lambda_2}e^{-\lambda_2|z-h|} + \dfrac{I^+(\xi)}{I^-(\xi)}\left[\dfrac{\vartheta_1}{\lambda_1}e^{-\lambda_1|z+h|} + \dfrac{\vartheta_2}{\lambda_2}e^{-\lambda_2|z+h|}\right] \\ - \dfrac{2}{I^-(\xi)}\left[\eta_2\nu_2\dfrac{\vartheta_1}{\lambda_2}e^{-(\lambda_1 z + \lambda_2 h)} + \eta_1\nu_1\dfrac{\vartheta_2}{\lambda_1}e^{-(\lambda_2 z + \lambda_1 h)}\right] \end{Bmatrix} \tag{37}$$

$$\gamma_1(\xi,z;h) = \frac{1}{2\left(\eta_1\lambda_2^2 - \eta_2\lambda_1^2\right)} \begin{Bmatrix} \lambda_1\vartheta_2 e^{-\lambda_1|z-h|} - \lambda_2\vartheta_1 e^{-\lambda_2|z-h|} - \dfrac{I^+(\xi)}{I^-(\xi)}\left[\lambda_1\vartheta_2 e^{-\lambda_1|z+h|} + \lambda_2\vartheta_1 e^{-\lambda_2|z+h|}\right] \\ + \dfrac{2}{I^-(\xi)}\left[\lambda_1\vartheta_1\eta_2\nu_2 e^{-(\lambda_1 z + \lambda_2 h)} + \lambda_2\vartheta_2\eta_1\nu_1 e^{-(\lambda_2 z + \lambda_1 h)}\right] \end{Bmatrix} \tag{38}$$

$$\gamma_3(\xi,z;h) = \frac{\alpha_3 c_{44}\xi}{2\alpha_2 c_{33}\left(\lambda_1^2 - \lambda_2^2\right)} \begin{Bmatrix} \mathrm{sgn}(z-h)\left(e^{-\lambda_1|z-h|} - e^{-\lambda_2|z-h|}\right) + \dfrac{I^+(\xi)}{I^-(\xi)}\left[e^{-\lambda_1|z+h|} + e^{-\lambda_2|z+h|}\right] \\ - \dfrac{2}{I^-(\xi)}\left[\eta_2\nu_2\dfrac{\lambda_1}{\lambda_2}e^{-(\lambda_1 z + \lambda_2 h)} + \eta_1\nu_1\dfrac{\lambda_2}{\lambda_1}e^{-(\lambda_2 z + \lambda_1 h)}\right] \end{Bmatrix} \tag{39}$$

$$\gamma_2(\xi,z;h) = \frac{1}{2\lambda_3}\left\{e^{-\lambda_1|z-h|} + e^{-\lambda_3|z+h|}\right\} \tag{40}$$

$$\eta_i = (\alpha_3 - \alpha_2)\lambda_i^2 + \xi^2(1+\alpha_1) - \frac{\rho_s\omega^2}{c_{66}}, \vartheta_i = \alpha_3\lambda_i^2 - \eta_i,$$
$$\nu_i = \left(\eta_i - \alpha_3\frac{c_{13}}{c_{33}}\xi^2 - \alpha_3\lambda_i^2\right)\lambda_i, i = 1,2 \tag{41}$$

$$I^{\pm}(\xi) = \eta_2\nu_1 \pm \eta_1\nu_2 \tag{42}$$

5. Interaction factors for partially embedded inclined piles

The application of the proposed analysis can be extended to the vibration of partially embedded piles. The superposition principle can be employed in which the dynamic stiffness of a group of piles can be determined by superposing the effect of two piles located at the arbitrary distance *s* from each other. The dynamic interaction factor under various modes of vibration are defined as (see Refs. [32,33])

$$\alpha = \frac{U_{21}}{U_{11}} \tag{43}$$

where U_{21} is the dynamic displacement of pile 2 caused by the dynamic excitation of pile 1; U_{11} is static displacement of pile 1 resulting from its own applied load. Displacement used here is to indicate the response of piles in either a translation or rotation mode. The dynamic interaction factors are obtained by applying a unit-amplitude harmonic load on first pile (source) and determining the displacements on the second pile (receiver), as shown in Fig. 5. The piles can have different inclination angle denoted by β_1 and β_2 in this figure.

The hybrid element method proposed for a single inclined pile can be extended to analyze two partially embedded inclined piles. A number of radiation discs subjected to vibrations are introduced for extended soil domain and the partially embedded inclined piles are discretized into N-1 elements as shown in Fig. 6. The stiffness of the pile group composed of two piles is written as

$$[K_P] = \begin{bmatrix} \left[K_{SP}^1\right]_{3N\times3N} & 0 \\ 0 & \left[K_{SP}^2\right]_{3N\times3N} \end{bmatrix}_{6N\times6N} \tag{44}$$

The dynamic flexibility matrix for a two-pile system can be formulated as

$$[C_S] = \begin{bmatrix} [C_{11}]_{3N\times3N} & [C_{12}]_{3N\times3N} \\ [C_{21}]_{3N\times3N} & [C_{22}]_{3N\times3N} \end{bmatrix}_{6N\times6N} \tag{45}$$

Here, C_{11} and C_{22} represent the dynamic flexibility matrices for pile 1 and pile 2, respectively, while C_{12} and C_{21} denote the dynamic flexibility matrices that consider the effect of pile 1 on pile 2 and vice versa. Similar to the formulation obtained for a single pile, the invert of soil's flexibility matrix will result in $[K_S]$, which need to be combined with pile stiffness matrix for the total stiffness matrix $[K_T]$.

6. Nnumerical solutions for dynamic stiffness matrix of the inclined pile

Since displacement compatibility between the pile and soil is enforced only at the pile's axis of symmetry, suitable load patterns must be applied at the radiation discs to ensure that the plane cross-sections of the pile remain nearly rigid and plane during deformation. Various types

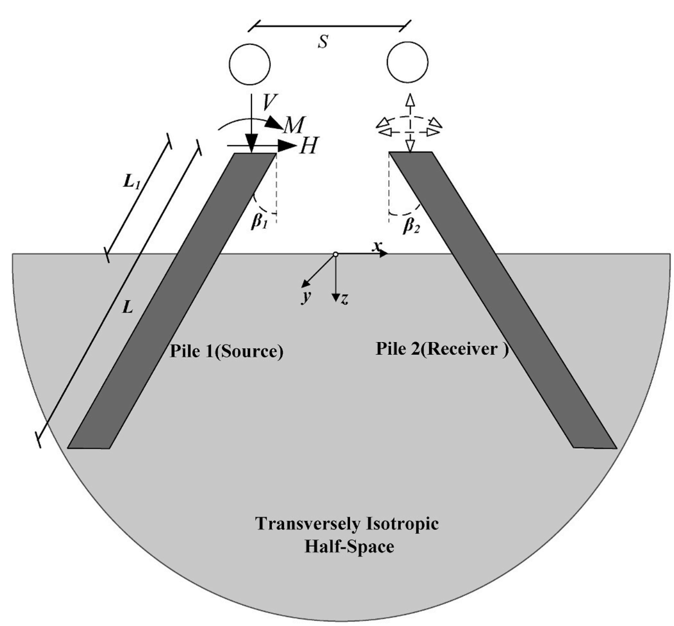

Fig. 5. Source-receiver piles under harmonic loading.

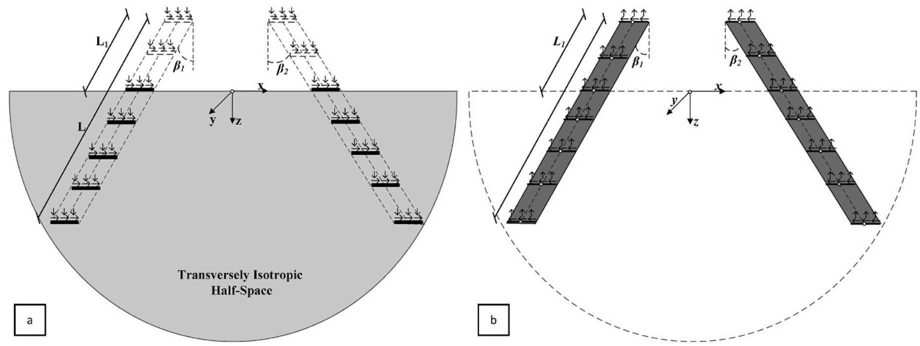

Fig. 6. The hybrid element method for partially embedded piles a) extended soil domain b) fictitious inclined piles.

of unit stress distributions can be defined on the radiation discs. Among these, a loading pattern following Boussinesq's model is assumed to act on the radiation discs to best represent high rigidity of the pile and to ensure full compatibility conditions at the cross-section of the pile. This load pattern with unit magnitude is mathematically written as

$$P(r,\theta)=\begin{cases}\cos(\theta)\Big/\left(2\pi a^2\sqrt{1-(r^2/a^2)}\right) & r<a\\ 0 \quad r\geq a\end{cases} \tag{46}$$

$$Q(r,\theta)=\begin{cases}-\sin(\theta)\Big/\left(2\pi a^2\sqrt{1-(r^2/a^2)}\right) & r<a\\ 0 \quad r\geq a\end{cases} \tag{47}$$

$$R(r,\theta)=\begin{cases}1\Big/\left(2\pi a^2\sqrt{1-(r^2/a^2)}\right) & r<a\\ 0 \quad r\geq a\end{cases} \tag{48}$$

The Boussinesq-type load distribution represents the stress distribution derived from the analytical solution for a rigid circular disc undergoing elastostatic vertical or lateral movement. Most previous studies have assumed a uniform load distribution to satisfy this compatibility condition, although this assumption may not hold even in elastostatic analyses. The impact of excitation frequency on the validity of the Boussinesq loading distribution beneath the radiation disc was discussed in detail by Shahbodagh et al. [29]. A unit load magnitude is considered to obtain the flexibility matrix for the soil. Imposing the angular Fourier expansion and the mth order Hankel transform to Equations (46)–(48) yields

$$X_m=\begin{cases}\sin(a\xi)/(2\pi a\xi) & m=+1\\ 0 \quad m\neq +1\end{cases} \tag{49}$$

$$Y_m=\begin{cases}\sin(a\xi)/(2\pi a\xi) & m=-1\\ 0 \quad m\neq -1\end{cases} \tag{50}$$

$$Z_m=\begin{cases}\sin(a\xi)/(2\pi a\xi) & m=0\\ 0 \quad m\neq 0\end{cases} \tag{51}$$

The flexibility matrix of the extended soil medium can be calculated by substituting Equations (49)–(51) into (34)–(35) and conducting numerical integration. An adaptive algorithm is employed for the integration taking into account the oscillatory behavior of the integrands. Also, there are several singularities in the path of integrations in terms of branch points and pole. The pole is isolated by finding the solution of equation $I(\xi_R)=0$, where ξ_R is related to the Rayleigh wave number. The other singular points belong to branch points existed in the kernel functions (36) to (40), which can be identified from $\lambda_i(\xi_{\lambda_i})=0, i=1,2,3$. The effect of the pole has been addressed with the aid of the theory of residuals in integration (see Ref. [39]). The contribution of Rayleigh pole across the small semi-circular boundary can be obtained using this theory as $-\pi i\mathrm{Res}(\xi_R)$, where $\mathrm{Res}(\xi_R)=\lim_{\xi\to\xi_R}[q(\xi)/(\mathrm{d}I(\xi)/\mathrm{d}\xi)]$. In this equation, $q(\xi)$ is an analytic function at ξ_R which can be obtained by rearranging the integrands in the form of $q(\xi)/I(\xi)$. The impedance functions for vibration of inclined pile can be written in a non-dimensional form as

$$\begin{Bmatrix}\overline{V}_0\\ \overline{H}_0\\ \overline{M}_0\end{Bmatrix}=\begin{bmatrix}K_{VV} & K_{VH} & K_{VM}\\ K_{HV} & K_{HH} & K_{HM}\\ K_{MV} & K_{MH} & K_{MM}\end{bmatrix}\begin{Bmatrix}\overline{u}_z(0)\\ \overline{u}_x(0)\\ \overline{\theta}_y(0)\end{Bmatrix} \tag{52}$$

where

$$\begin{gathered}\overline{z}=z\big/a, \overline{u}_z(\overline{z})=u_z^f(z)\big/a, \overline{u}_x(\overline{z})=u_x^f(z)\big/a, \overline{\theta}_y(\overline{z})=\theta_y^f(z),\\ \overline{M}_0=M_0\big/(8E_s'a^3), \overline{H}_0=H_0\big/(4E_s'a^2), \overline{V}_0=V_0\big/(4E_s'a^2),\end{gathered} \tag{53}$$

$u_z^f(z)$, $u_x^f(z)$ and $\theta_y^f(z)$ are vertical deformation, the lateral deformation, and the rotation of the pile under combined vertical loading (V_0), lateral loading (H_0) and bending moment (M_0) imposed at the head of the pile. The impedance functions are frequency-dependent and represented by complex numbers. They are usually expressed as $K_{ij}=k_{ij}+i\omega_0 c_{ij}$, where k_{ij} and c_{ij} are the dynamic stiffness and damping matrices, and ω_0 is a non-dimensional frequency. In the presented study, ω_0 is defined as $\omega_0=\omega a\sqrt{\rho_s/c_{44}}$.

The analytical–numerical solution has been implemented in MATLAB. Custom scripts were developed for both the finite element analysis of the piles and the numerical integration required for the radiation disc formulation. The algorithms were optimized to ensure computational efficiency and accuracy.

6.1. Convergence of the method

In the proposed solution, radiation discs are used to represent the interaction of the pile with the homogeneous transversely isotropic half-space. This section examines how the number of radiation discs impacts the accuracy of the solution. Fig. 7 illustrates the magnitude of the error in the horizontal and vertical impedance functions for different pile inclination angles and $\omega_0=0.5$, in relation to the number of radiation discs used along the length of the inclined pile. The mechanical properties of the pile-soil system are $\rho_P/\rho_S=1.43$, $L_p/a=30$, $E_P/E_S'=1000$, $G_S/G_S'=2$. The material properties for soil are indicated in Table 1 and denoted by Material 4. It should be noted that the errors of calculation are computed with respect to the converged solution with $N=100$ for all the cases considered.

As observed, increasing the number of radiation discs leads to a high rate of convergence. The convergence rate of the vertical mode of vibration is higher compared to that of the horizontal mode. This difference is due to the greater complexity of the governing equations for the horizontal modes of vibration, including the asymmetric vibration of radiation discs and higher-order governing equations for pile vibration. For an inclined pile under lateral vibration, the inclination angle increases the contribution of the vertical mode, thus increasing the solution accuracy. Conversely, increasing the pile inclination angle negatively impacts the vertical mode of vibration, as it introduces

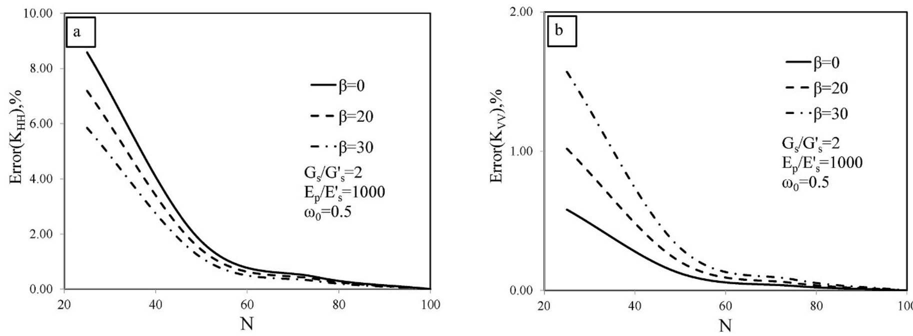

Fig. 7. The magnitude of errors for the impedance functions with respect to the number of radiation discs for $\omega_0 = 0.5$: a) horizontal mode, b) vertical mode.

Table 1
Material properties for the transversely isotropic soil.

Material	E_S	E'_S	G'_S	ν_S, ν'_S	Anisotropy degree
1[I]	5.0	5.0	2.0	0.25	$G_S/G'_S = E_S/E'_S = 1$
2[T]	10.0	5.0	2.0	0.25	$E_S/E'_S = 2$
3[T]	15.0	5.0	2.0	0.25	$E_S/E'_S = 3$
4[T]	5.0	5.0	1.0	0.25	$G_S/G'_S = 2$
5[T]	5.0	5.0	0.7	0.25	$G_S/G'_S = 3$

[I] Isotropic, [T] Transversely isotropic.
Note: All parameters are in GPa, except for the Poisson's ratios, which are dimensionless.

asymmetry within the system. To demonstrate the effect of excitation frequency on the magnitude of error, the errors in the impedance functions are also evaluated for high-frequency excitation of $\omega_0 = 1$, as shown in Fig. 8. This figure shows a slight reduction in the convergence rate compared to low-frequency excitation, while maintaining the overall trend of Fig. 7. It is important to highlight that $\omega_0 = 1$ represents a very high non-dimensional frequency in geotechnical applications. Many previous studies have also considered this as the upper bound in their analysis.

6.2. The validation of numerical solutions

This section validates the reliability and the accuracy of the presented solutions. The dynamic response of an inclined pile buried in an isotropic half-space is examined and compared to existing analytical and numerical solutions. The analysis considers a fixed-head pile under various loading (i.e. vertical, horizontal, and bending). The static lateral stiffness of an inclined pile with $L_p/a = 30$, $E_P/E'_S = 100, 1000$ and $\nu_s = 0.4$ are depicted in Fig. 9. The results are presented along with the analytical solution reported by Poulos and Davis [1] and numerical solutions obtained using the BEM-FEM method by Padron et al. [5]. Good agreements are observed between the presented solution and the existing analytical and numerical solutions. The gradual increase in lateral stiffness with respect to the pile inclination angle is evident, which is attributed to the mobilization of vertical stiffness.

The dynamic impedance of an inclined pile in homogenous isotropic half-space are also generated for the previous pile by assuming $\rho_P/\rho_S = 1.43$ and compared with the results reported by Padron et al. [5]. In order to compare the results, a damping coefficient of $\overline{\beta}_s = 0.05$ is also considered for the isotropic half-space. Fig. 10 demonstrates the lateral impedance functions of the inclined pile with inclination angles of $\beta = 20^\circ, 30^\circ$. Due to the moderate nonlinearity of the impedance function with respect to vibration frequency, a frequency interval of 0.05 is selected to effectively capture and demonstrate their frequency-dependent characteristics. It can be seen that excelent predictions are achieved using the hybrid element method. The vertical impedence functions are also obtained and depicted in Fig. 11. At high frequency, it is seen that the presented results slightly deviate from the BEM-FEM solutions for the stiff pile with $E_P/E'_S = 1000$. The rocking and

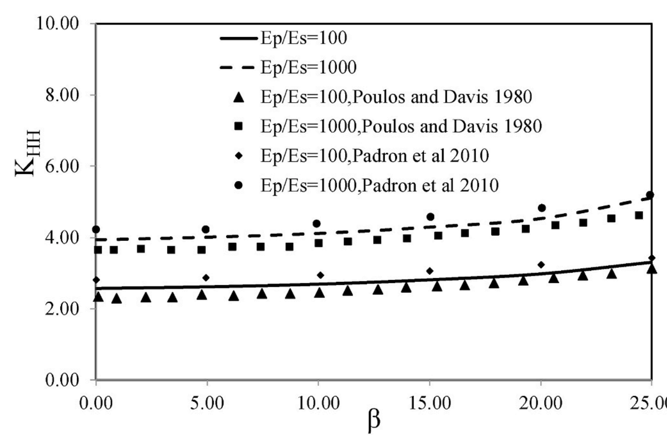

Fig. 9. The static horizontal stiffness of an inclined pile embedded in isotropic soil.

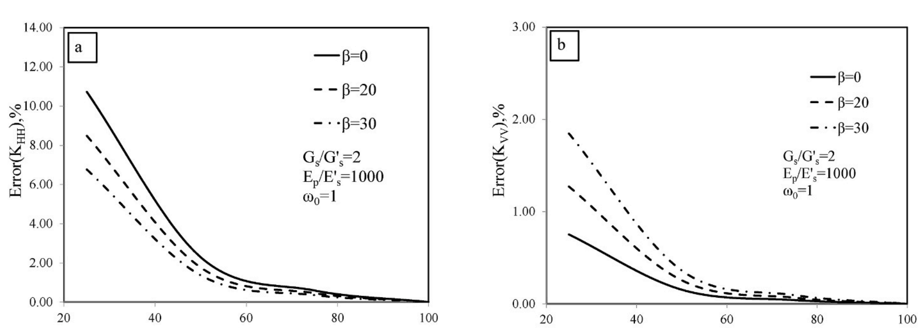

Fig. 8. The magnitude of errors for the impedance functions with respect to the number of radiation discs for $\omega_0 = 1$: a) horizontal mode, b) vertical mode.

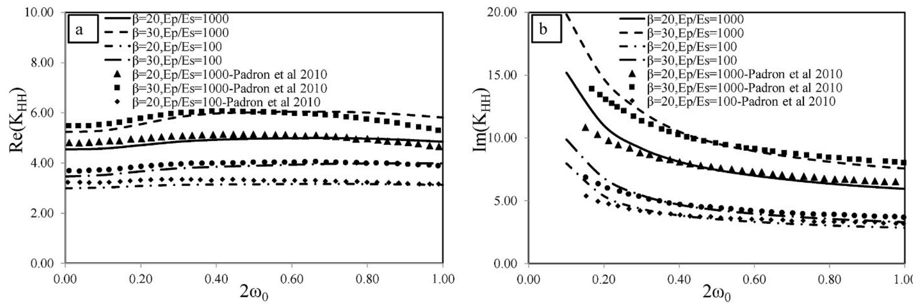

Fig. 10. The horizontal impedance of an inclined pile embedded in isotropic soil vs the excitation frequency: a) real part, b) imaginary part.

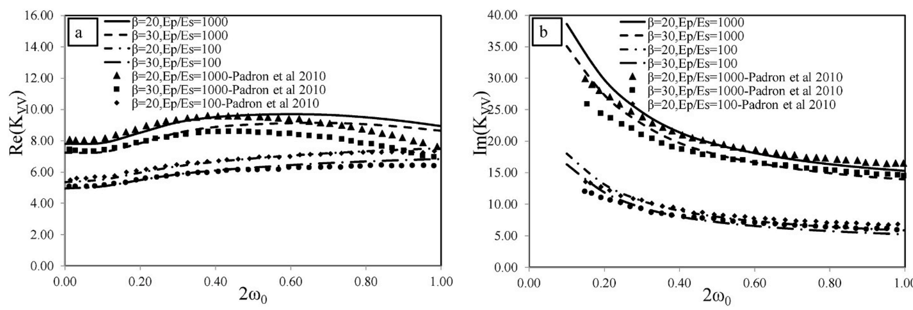

Fig. 11. The vertical impedance of an inclined pile embedded in isotropic soil vs the excitation frequency: a) real part, b) imaginary part.

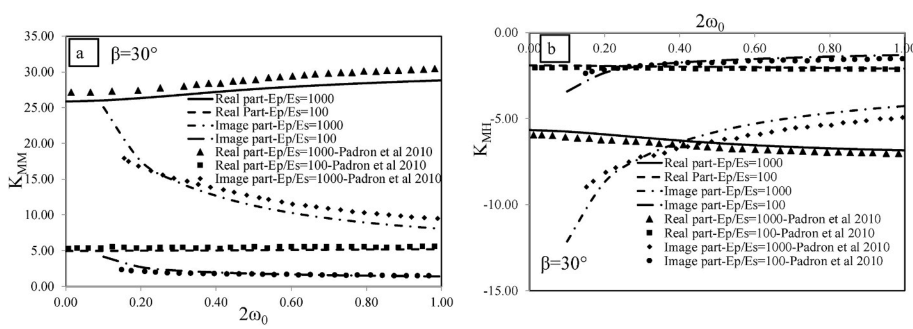

Fig. 12. The impedance functions under the rotational vibrations: a) rocking mode, b) coupling mode.

the coupling impedance functions are provided in Fig. 12 for an inclined pile with $\beta = 20^{\circ}$. Less agreement is also observed for the case with $E_P/E_S' = 1000$, similar to the vertical impedance solution. The discrepancies observed in Figs. 11 and 12 can be attributed to the different assumptions made between the present work and Padron et al. [5]. In the present study, the radiation condition is analytically enforced across all dimensions of the model. However, the discretization of the boundary surface in Pedron et al. [5] may affect the accurate satisfaction of the radiation condition. In addition, Padron's study enforces non-nodal collocation points at different locations around the perimeter of the pile in their FEM modeling, while in the present work, a Boussinesq-type loading is applied to ensure that the pile's cross-sections remain nearly rigid and plane during deformation.

To validate the numerical procedure proposed for a group of two piles, the dynamic interaction factors for vertical piles buried in homogeneous soils are evaluated and compared with the existing solutions reported by Kaynia [32]. The material parameters for soil and piles are selected as $L_P/a = 30$, $\rho_P/\rho_S = 1.43$, $E_P/E_S' = 1000$, $\nu_s = 0.4$ and $\overline{\beta}_s = 0.05$. The vertical, lateral, and rocking interaction factors are calculated

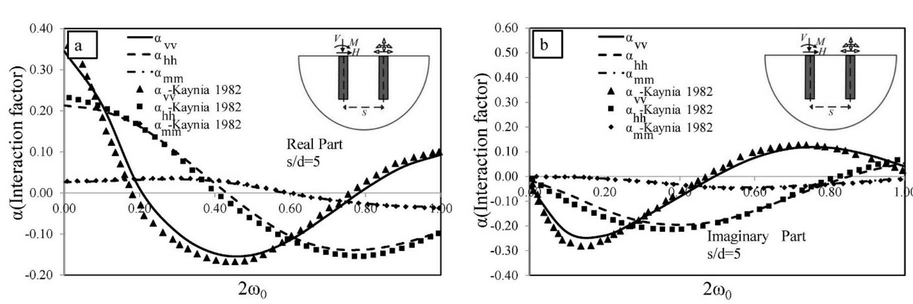

Fig. 13. Dynamic interaction factors for vertical piles in homogenous soil: a) real part b) imaginary part.

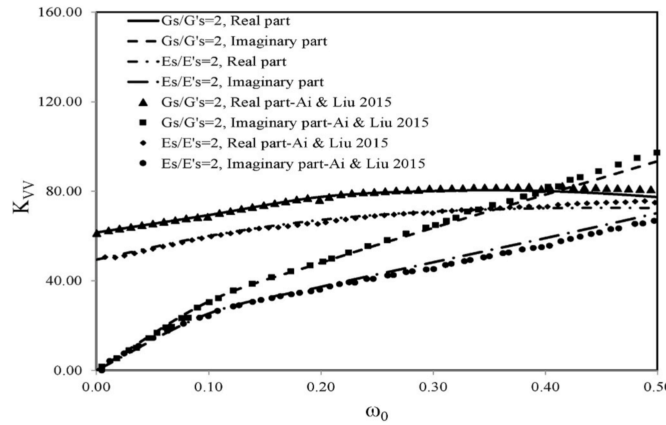

Fig. 14. The vertical impedance of a vertical pile embedded in transversely isotropic soil.

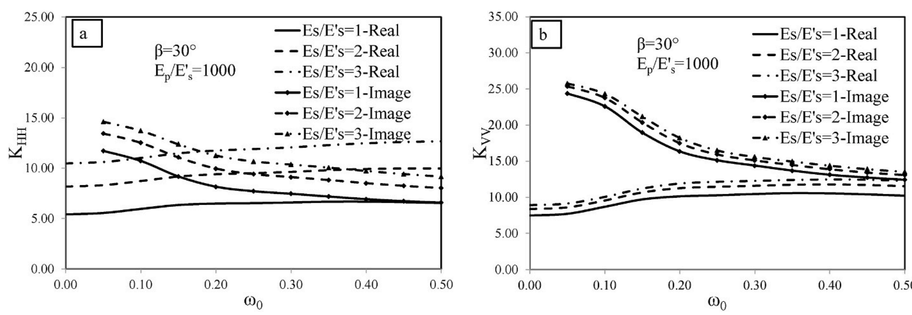

Fig. 15. Dynamic impedance of the inclined pile (β = 30°) in transversely isotropic half-space with ascending E_S/E_S' values: a) horizontal mode, b) vertical mode.

by means ofhybrid element method, as shown in Fig. 13 demonstrating satisfactory agreement with the solutions provided by Kaynia [32].

The accuracy of the presented framework in capturing the dynamic behavior of piles in anisotropic soils is assessed through comparison with existing benchmark solutions. To this end, the impedance of a vertical pile embedded in a transversely isotropic half-space is compared with the results reported by Ai and Liu [40]. A vertical pile with $\rho_P/\rho_S = 1.5$, $E_P/E_S' = 500$, $L_p/a = 40$ and $\overline{\beta}_s = 0$ is considered. Table 1 presents the material parameters (Materials 2 and 4) considered for the transversely isotropic half-space. Note that $K_{ij} = k_{ij} + ic_{ij}$ is assumed for the impedance function in Fig. 14, consistent with the assumption used by Ai and Liu [40]. Excellent agreement is observed between the two results, validating the capability of the proposed model in capturing the dynamic behavior of piles in anisotropic soil media.

6.3. The behavior of an inclined pile in transversely isotropic half-space

To investigate how material anisotropy affects the behavior of an inclined pile, various materials are selected for a transversely isotropic half-space, as shown in Table 1. Here, an inclined pile with $\rho_P/\rho_S = 1.43$, $L_p/a = 30$ and $\overline{\beta}_s = 0$ are selected. The vertical and horizontal impedance functions for an inclined pile with β = 30° are obtained for various transversely isotropic materials, as shown in Figs. 15 and 16. Similarly, these functions are determined for a vertical pile, i.e. β = 0°, and presented in Figs. 17 and 18. In these figures, the degree of anisotropy varies relative to a reference isotropic material (Mat. 1). As shown in Figs. 15 and 16, the impedance functions for anisotropic cases increase relative to the isotropic case as E_S increases. Additionally, the reduction of the out-of-plane shear modulus (G_S') significantly decreases the magnitude of the impedance functions, as noted in Fig. 16. Unlike the inclined pile, Figs. 17 and 18 show that E_S has minimal impact on the vertical impedance functions (Fig. 17b). This highlights that soil anisotropy in vertical and horizontal directions can markedly affect the dynamic behavior of an inclined pile as the inclined orientation makes the pile more sensitive to the directional properties of the surrounding soil.

Figs. 19–21 demonstrate the lateral, vertical, and rocking impedance functions of an inclined pile with different inclination angles and pile stiffness ratios. Similar to the behavior of an inclined pile embedded in isotropic materials, an increase in dynamic stiffness is observed with increasing inclination angles and pile stiffness ratios for piles embedded in anisotropic materials. Most notably, as seen in Fig. 19, the change in pile inclination angle has a significant impact on the dynamic behavior of the inclined piles embedded in anisotropic soils with varying G_S' values. Fig. 21 shows that the rocking mode of vibration is less affected by the pile inclination angle, especially for flexible inclined piles.

The effect of soil anisotropy on the dynamic interaction factors of inclined piles is investigated here. Figs. 22 and 23 illustrate the vertical and lateral dynamic interaction factors for inclined piles buried in a transversely isotropic material ($G_S/G_S' = 2$). Here it is assumed pile-soil material parameters are $E_P/E_S' = 1000$, $\rho_P/\rho_S = 1.43$, $L_p/a = 30$ and $\overline{\beta}_s = 0$. The impact of changing the pile inclination angle on the interaction factor is more significant in the vertical mode, where the receiver pile shows reduced vertical deformation as the inclination angle increases. For the lateral interaction factor, the shift from lateral to vertical loading also results in a drop in the lateral deformation of the

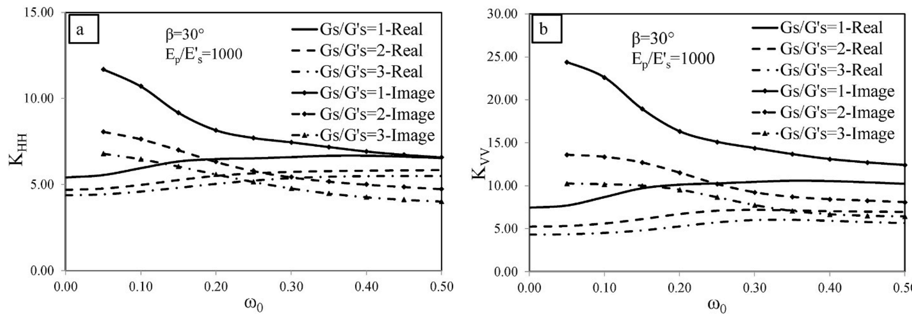

Fig. 16. Dynamic impedance of the inclined pile (β = 30°) in transversely isotropic half-space with descending G_S/G_S' values: a) horizontal mode, b) vertical mode.

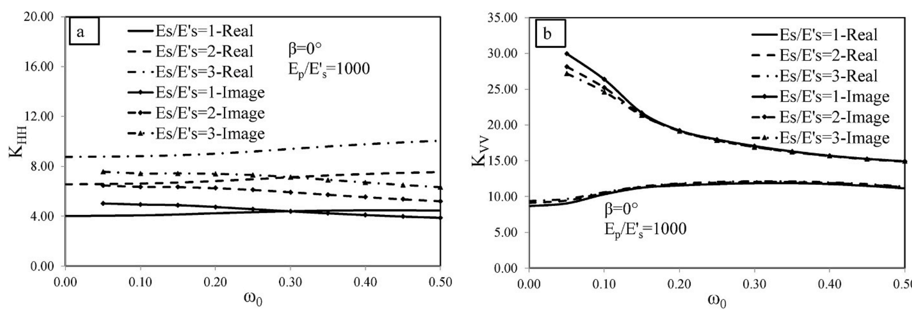

Fig. 17. Dynamic impedance functions of a vertical pile in transversely isotropic half-space with ascending E_S/E_S' variation: a) horizontal mode, b) vertical Mode.

receiver inclined pile, as illustrated in Fig. 23.

In many practical scenarios, inclined piles can be partially embedded in soil. This section explores the impact of partial embedment on the interaction factors for inclined piles with different embedment ratios (L_1/L) in a transversely isotropic soil ($G_S/G_S' = 2$). For vertical piles, the vertical and lateral interaction factors are presented in Fig. 24. An increase in the embedment ratio has a minimal effect on the vertical interaction factors but significantly alters the lateral interaction factor, indicating reduced translation in the receiver pile. In contrast, for inclined piles, both lateral and vertical interaction factors are affected by the embedment ratio, as shown in Fig. 25.

The interaction factor can get negative values in both the real and imaginary parts, representing the out of phase response of the piles (see Refs. [41,42]). Negative values in the real part indicate that the displacement of the affected pile is in the opposite direction to the loading on the source pile. The negative imaginary part is associated with a phase lag between the response of the affected pile and the source pile, representing significant damping effects in the soil-pile system (see Ref. [43]). In soil dynamics, in general, the imaginary part of response has particular significance as it characterizes the attenuation of the waves and energy dissipation mechanisms within the soil medium [44, 45].

7. Conclusions

A hybrid analytical-numerical framework was presented to explore the dynamic response of inclined piles embedded in transversely isotropic media. A set of complete displacement potential functions, along with the Fourier series and Hankel transforms, were used to obtain the fundamental Green's functions for the transversely isotropic half-space. The dynamic Euler-Bernoulli beam theory was employed to model the inclined piles under vibrations. The exact solutions of the beam were used to establish the frequency-dependent stiffness matrix of the inclined pile under lateral, vertical, and rocking modes of vibrations. The compatibility of displacements between the inclined pile and soil was enforced at nodal points defined along the pile length. A series of radiation discs, whose solutions obtained using the Green's functions, were introduced at the nodal points to model the dynamic soil-pile interaction. The mathematical framework was expanded to address the vibration of two partially embedded inclined piles, allowing for the calculation of dynamic interaction factors. These factors can be utilized to understand the behavior of pile groups containing inclined piles using the superposition principle. The model was validated by comparing the static and dynamic impedance functions with the existing numerical and analytical solutions for isotropic soils. Good agreement was seen between the simulation results and the existing solutions in all the cases

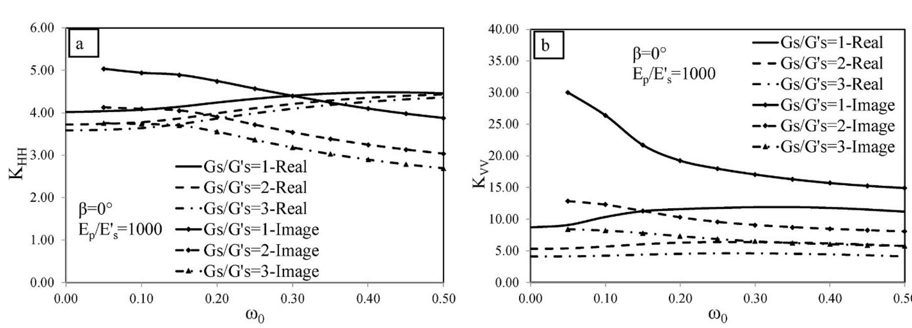

Fig. 18. Dynamic impedance functions of a vertical pile in transversely isotropic half-space with G_S/G_S' variation: a) horizontal mode, b) vertical mode.

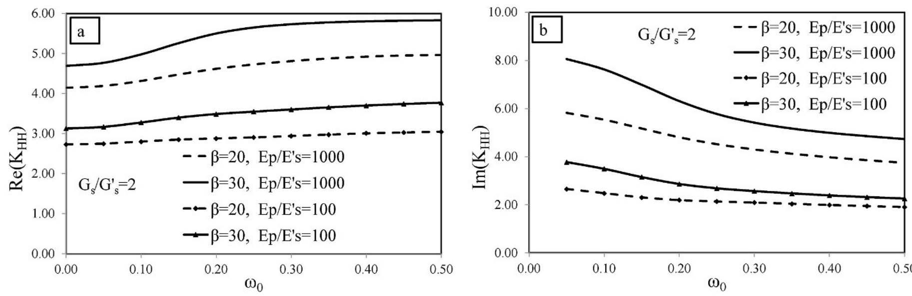

Fig. 19. Horizontal dynamic impedance of inclined piles with $G_S/G'_S = 2$ and various inclination angles: a) real part, b) imaginary part.

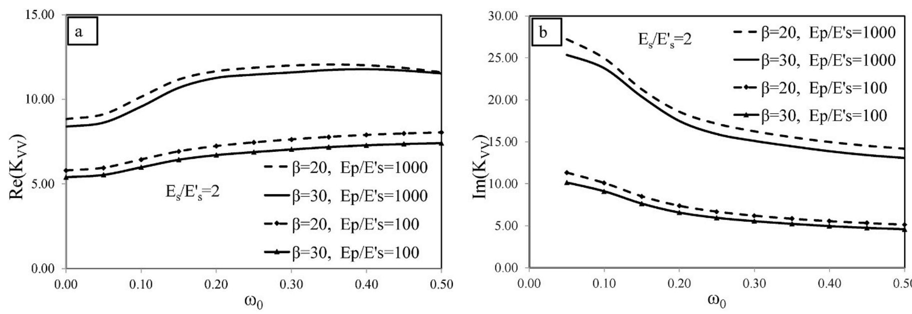

Fig. 20. Vertical dynamic impedance of inclined piles with $E_S/E'_S = 2$ and various inclination angles: a) real part, b) imaginary part.

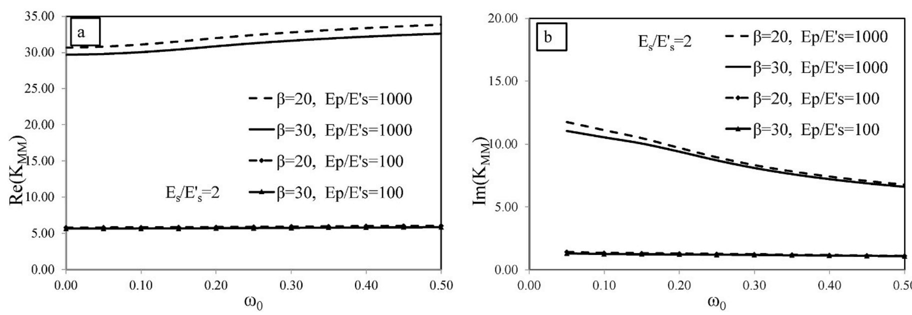

Fig. 21. Rocking dynamic impedance of inclined piles with $E_S/E'_S = 2$ and various inclination angles: a) real part, b) imaginary part.

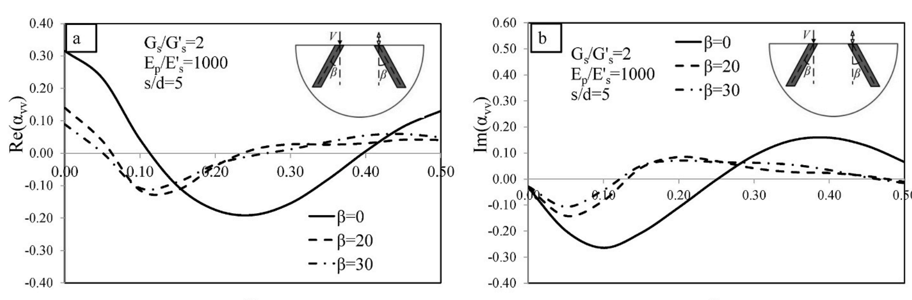

Fig. 22. The vertical interaction factors for inclined piles in transversely isotropic soil a) real part b) imaginary part.

considered. It was demonstrated that soil anisotropy can markedly influence the dynamic behavior of inclined piles, while it only alters the impedance functions of vertical piles at specific anisotropy degrees and loading conditions. Increasing the inclination angle and pile stiffness ratio leads to a rise in impedance functions for piles subject to horizontal loading in transversely isotropic materials, similar to the behavior observed in inclined piles embedded in isotropic soils. This study adopts elastodynamic theory, assuming linear elastic behavior for soil and pile with fully bonded contact at pile-soil interface. These assumptions are valid for practical pile vibration problems where vibration amplitude remains low, such as in machine foundations (see Refs. [46,47]). It has also been shown that Boussinesq-type loading preserves the rigid deformation of the pile cross-section at moderate vibration frequencies, while a frequency-dependent loading pattern can extend this rigidity across a wider range. Additionally, the Euler-Bernoulli beam theory, primarily applicable to slender piles, was adopted. However, for inclined piles with a low slenderness ratio, more advanced beam theories, such as Timoshenko's theory (see Ref. [8]), should be employed to account for

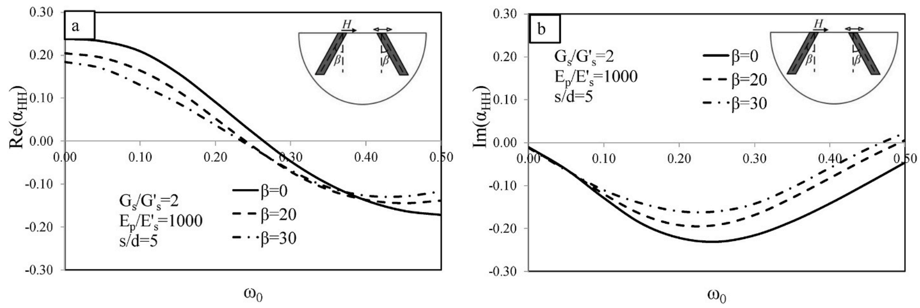

Fig. 23. The lateral interaction factors for inclined piles in transversely isotropic soil a) real part b) imaginary part.

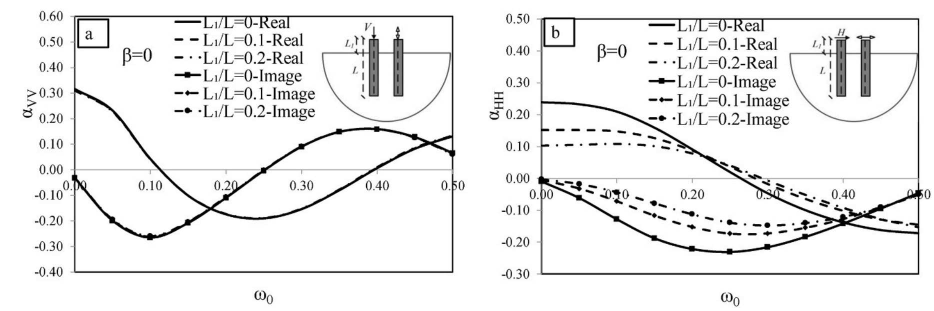

Fig. 24. Dynamic interaction factors for partially embedded vertical piles in transversely isotropic soil under a) vertical mode b) lateral mode of vibrations.

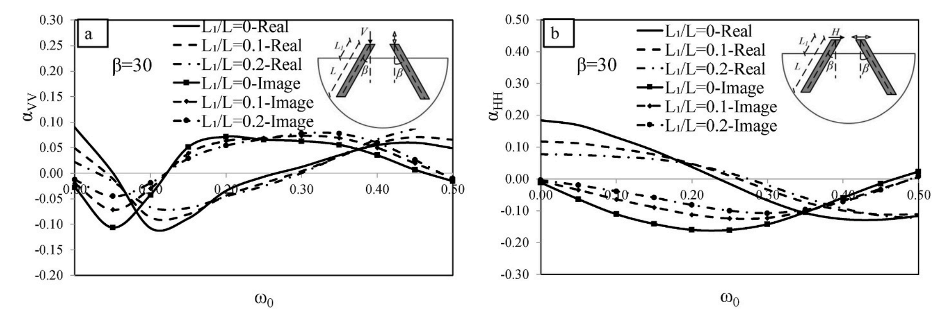

Fig. 25. Dynamic interaction factors for partially embedded inclined piles in transversely isotropic soil under a) vertical mode b) lateral mode of vibrations.

shear deformation and rotational inertia.

CRediT authorship contribution statement

Hamed Moghaddasi: Writing – review & editing, Writing – original draft, Validation, Methodology, Investigation, Formal analysis, Conceptualization. **Babak Shahbodagh:** Writing – review & editing, Validation, Methodology, Investigation, Conceptualization. **Ali Khojasteh:** Writing – review & editing, Methodology, Conceptualization. **Mohammad Rahimian:** Writing – review & editing, Supervision, Methodology, Conceptualization.

Declaration of competing interest

The authors declare that they have no known competing financial interests or personal relationships that could have appeared to influence the work reported in this paper.

Appendix A

A fictitious inclined pile is considered in the local coordinate system, as shown in Fig. A1. For an infinitesimal element of the pile with length $d\overline{z}$ and mass $dm = \rho_e A_P d\overline{z}$, the equations governing the vertical and horizontal motions of the element can be written in the local coordinate system (see Fig. A1)

$$\frac{\partial \overline{V}(\overline{z},t)}{\partial \overline{z}} + \rho_e A_P \frac{\partial^2 \overline{y}(\overline{z},t)}{\partial t^2} = 0 \tag{A1}$$

$$\frac{\partial \overline{F}(\overline{z},t)}{\partial \overline{z}} + \rho_e A_P \frac{\partial^2 \overline{w}(\overline{z},t)}{\partial t^2} = 0 \tag{A2}$$

where the local axial and shear forces are denoted by $\overline{V}(\overline{z},t)$ and $\overline{F}(\overline{z},t)$, respectively. The moment equilibrium for the element can also be invoked which results in bending moment relationship as $\overline{M}(\overline{z},t) = \frac{\partial \overline{V}(\overline{z},t)}{\partial \overline{z}}$. For small deformations in the inclined pile, the bending moment is correlated to the deflection by $\overline{M}(\overline{z},t) = E_e I_p \frac{\partial^2 \overline{y}(\overline{z},t)}{\partial \overline{z}^2}$ and the local axial force can be linked to local vertical displacement by $\overline{F}(\overline{z},t) = E_e A_P \frac{\partial \overline{w}(\overline{z},t)}{\partial \overline{z}}$. Substituting these equations into the lateral and vertical motion equations (A1) and (A2) results in the governing equations for the local displacements, presented in Equations (8) and (9).

The dynamic stiffness matrix for the inclined pile is calculated based on the classical Bernoulli-Euler beam theory. Through the analytical solution of the equations of motion (8) and (9) and the imposition of the endpoint boundary conditions, the stiffness of the beam-column element in the local coordinate system (as shown in Fig. A2) is obtained as

$$\begin{Bmatrix} \overline{F}_1 \\ \overline{V}_1 \\ \overline{M}_1 \\ \overline{F}_2 \\ \overline{V}_2 \\ \overline{M}_2 \end{Bmatrix} = \begin{bmatrix} \gamma\Lambda_7 H & 0 & 0 & -\gamma H & 0 & 0 \\ 0 & -\alpha^3\Lambda_1 D & -\alpha^2\Lambda_2 D & 0 & \alpha^3\Lambda_4 D & \alpha^2\Lambda_5 D \\ 0 & -\alpha^2\Lambda_2 D & \alpha\Lambda_3 D & 0 & -\alpha^2\Lambda_5 D & -\alpha\Lambda_6 D \\ -\gamma H & 0 & 0 & \gamma\Lambda_7 H & 0 & 0 \\ 0 & \alpha^3\Lambda_4 D & -\alpha^2\Lambda_5 D & 0 & -\alpha^3\Lambda_1 D & \alpha^2\Lambda_2 D \\ 0 & \alpha^2\Lambda_5 D & \alpha\Lambda_6 D & 0 & \alpha^2\Lambda_2 D & \alpha\Lambda_3 D \end{bmatrix} \begin{Bmatrix} \overline{w}_1 \\ \overline{y}_1 \\ \overline{\theta}_1 \\ \overline{w}_2 \\ \overline{y}_2 \\ \overline{\theta}_2 \end{Bmatrix} \tag{A3}$$

where

$$\boldsymbol{\alpha} = \sqrt{\frac{\omega^2 \rho_e A_P}{E_e I_P}}, \gamma = \sqrt{\frac{\omega^2 \rho_e}{E_e}}$$

$$\boldsymbol{D} = \frac{E_e I_P}{\cos(\alpha L)\cosh(\alpha L) - 1}, H = \frac{E_e A}{\sin(\gamma L)}$$

$$\begin{aligned} &\Lambda_1 = \cos(\alpha L)\sinh(\alpha L) + \sin(\alpha L)\cosh(\alpha L), \Lambda_2 = \sin(\alpha L)\sinh(\alpha L) \\ &\Lambda_3 = \cos(\alpha L)\sinh(\alpha L) - \sin(\alpha L)\cosh(\alpha L), \Lambda_4 = \sin(\alpha L) + \sinh(\alpha L) \\ &\Lambda_5 = \cos(\alpha L) - \cosh(\alpha L), \Lambda_6 = \sin(\alpha L) - \sinh(\alpha L), \Lambda_7 = \cos(\gamma L) \end{aligned} \tag{A4}$$

$\overline{F}_i$, $\overline{V}_i$, and $\overline{M}_i$ ($i = 1,2$) are the internal axial and shear forces and bending moments, and $\overline{w}_i$, $\overline{y}_i$, and $\overline{\theta}_i$ are the associated vertical deformations, lateral deflections, and rotations at the nodes of the beam element, respectively. The force-displacement relation in the global coordinate system can be expressed as

$$\begin{Bmatrix} F_1 \\ V_1 \\ M_1 \\ F_1 \\ V_1 \\ M_1 \end{Bmatrix} = [T]^T \begin{bmatrix} \gamma\Lambda_7 H & 0 & 0 & -\gamma H & 0 & 0 \\ 0 & -\alpha^3\Lambda_1 D & -\alpha^2\Lambda_2 D & 0 & \alpha^3\Lambda_4 D & \alpha^2\Lambda_5 D \\ 0 & -\alpha^2\Lambda_2 D & \alpha\Lambda_3 D & 0 & -\alpha^2\Lambda_5 D & -\alpha\Lambda_6 D \\ -\gamma H & 0 & 0 & \gamma\Lambda_7 H & 0 & 0 \\ 0 & \alpha^3\Lambda_4 D & -\alpha^2\Lambda_5 D & 0 & -\alpha^3\Lambda_1 D & \alpha^2\Lambda_2 D \\ 0 & \alpha^2\Lambda_5 D & \alpha\Lambda_6 D & 0 & \alpha^2\Lambda_2 D & \alpha\Lambda_3 D \end{bmatrix} [T] \begin{Bmatrix} w_1 \\ y_1 \\ \theta_1 \\ w_2 \\ y_2 \\ \theta_2 \end{Bmatrix} \tag{A5}$$

where

$$[T] = \begin{bmatrix} \mathrm{Cos}(\beta) & -\mathrm{Sin}(\beta) & 0 & 0 & 0 & 0 \\ \mathrm{Sin}(\beta) & \mathrm{Cos}(\beta) & 0 & 0 & 0 & 0 \\ 0 & 0 & 1 & 0 & 0 & 0 \\ 0 & 0 & 0 & \mathrm{Cos}(\beta) & -\mathrm{Sin}(\beta) & 0 \\ 0 & 0 & 0 & \mathrm{Sin}(\beta) & \mathrm{Cos}(\beta) & 0 \\ 0 & 0 & 0 & 0 & 0 & 1 \end{bmatrix} \tag{A6}$$

The stress-displacement relation for the inclined pile element can be arranged as $[F] = [K]_P^e[\Delta]$, where $[F]$ and $[\Delta]$ are forces and displacements at the nodal points in the global coordinate system, and $[K]_P^e$ is the dynamic stiffness of the pile element. Similar to the finite element procedure, the dynamic stiffness matrices obtained for pile elements are assembled to form the overall stiffness matrix for the whole inclined pile. The stiffness matrix of a single pile with N-1 elements can be constructed by assembling the element stiffness matrices as

$$[K_P] = \begin{bmatrix} [K_{11}] & [K_{12}] & & & \\ [K_{12}] & [K_{11}] + [K_{22}] & & 0 & \\ & & \ddots \quad \ddots & & \\ & & \ddots \quad \ddots & & \\ & 0 & & [K_{11}] + [K_{22}] & [K_{12}] \\ & & & [K_{12}] & [K_{22}] \end{bmatrix}_{3N \times 3N} \tag{A7}$$

where $[K_{11}]$, $[K_{12}]$, $[K_{21}]$ and $[K_{22}]$ are the components of the stiffness matrix in each element, i.e.

$$[K]_P^e = \begin{bmatrix} [K_{11}] & [K_{12}] \\ [K_{21}] & [K_{22}] \end{bmatrix}_{6 \times 6} \tag{A8}$$

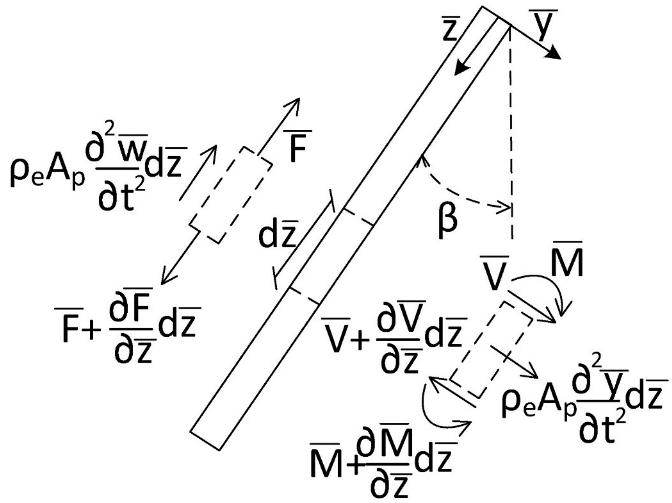

Fig. A1. An infinitesimal element of an inclined pile under force and moment equilibrium

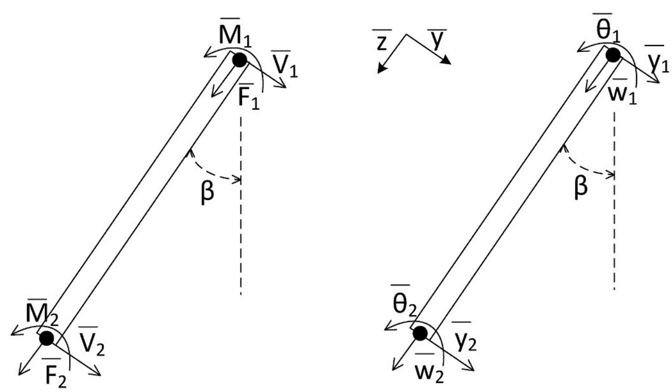

Fig. A2. The beam-column element in the local coordinate system: a) the nodal moments and forces, b) the nodal rotations and displacements.

Data availability

Data will be made available on request.

References

[1] Poulos HG, Davis EH. Pile foundation analysis and design, vol. 397. New York: Wiley; 1980. p. 233–48.
[2] Mamoon SM, Kaynia AM, Banerjee PK. Frequency domain dynamic analysis of piles and pile groups. J Eng Mech 1990;116(10):2237–57.
[3] Giannakou A, Gerolymos N, Gazetas G. On the dynamics of inclined piles. In: 10th international conference on piling and deep foundations; 2006. p. 286–95. Amsterdam.
[4] Gerolymos N, Giannakou A, Anastasopoulos I, Gazetas G. Evidence of beneficial role of inclined piles: observations and summary of numerical analyses. Bull Earthq Eng 2008;6:705–22.
[5] Padrón LA, Aznárez JJ, Maeso O, Santana A. Dynamic stiffness of deep foundations with inclined piles. Earthq Eng Struct Dynam 2010;39(12):1343–67.
[6] Giannakou A, Gerolymos N, Gazetas G, Tazoh T, Anastasopoulos I. Seismic behavior of batter piles: elastic response. J Geotech Geoenviron Eng 2010;136(9):1187–99.
[7] Ghasemzadeh H, Alibeikloo M. Pile–soil–pile interaction in pile groups with batter piles under dynamic loads. Soil Dynam Earthq Eng 2011;31(8):1159–70.
[8] Wang J, Zhou D, Ji T, Wang S. Horizontal dynamic stiffness and interaction factors of inclined piles. Int J GeoMech 2017;17(9):04017075.
[9] Carbonari S, Morici M, Dezi F, Gara F, Leoni G. Soil-structure interaction effects in single bridge piers founded on inclined pile groups. Soil Dynam Earthq Eng 2017;92:52–67.
[10] Rajeswari JS, Sarkar R. A three-dimensional investigation on performance of batter pile groups in laterally spreading ground. Soil Dynam Earthq Eng 2021;141:106508.
[11] Pak RY, Jennings PC. Elastodynamic response of pile under transverse excitations. J Eng Mech 1987;113(7):1101–16.
[12] Pak RYS. On the flexure of a partially embedded bar under lateral loads. J Appl Mech 1989;56:263–9.
[13] Rajapakse RKND, Shah AH. On the lateral harmonic motion of an elastic bar embedded in an elastic half-space. Int J Solid Struct 1987;23(2):287–303.
[14] Liu X, El Naggar MH, Wang K, Wu W. Dynamic soil resistance to vertical vibration of pipe pile. Ocean Eng 2021;220:108381.
[15] Ai ZY, Liu CL. Dynamic impedance of a pipe pile in layered soils under vertical excitations. Soil Dynam Earthq Eng 2017;97:387–94.
[16] Makris N, Gazetas G. Dynamic pile-soil-pile interaction. Part II: lateral and seismic response. Earthq Eng Struct Dynam 1992;21(2):145–62.
[17] Medina C, Padrón LA, Aznárez JJ, Santana A, Maeso O. Kinematic interaction factors of deep foundations with inclined piles. Earthq Eng Struct Dynam 2014;43(13):2035–50.
[18] Medina C, Padrón LA, Aznárez JJ, Maeso O. Influence of pile inclination angle on the dynamic properties and seismic response of piled structures. Soil Dynam Earthq Eng 2015;69:196–206.
[19] Wang Y, Rajapakse N. BE analysis of dynamics of rigid foundations embedded in transversely isotropic soils. J Chin Inst Eng 2000;23(3):275–88.
[20] Barros PLA. Impedances of rigid cylindrical foundations embedded in transversely isotropic soils. Int J Numer Anal Methods GeoMech 2006;30(7):683–702.
[21] Shahmohamadi M, Khojasteh A, Rahimian M, Pak RYS. Dynamics of a cylindrical pile in a transversely isotropic half-space under axial excitations. J Eng Mech 2013;139(5):568–79.
[22] Gharahi A, Rahimian M, Eskandari-Ghadi M, Pak RYS. Dynamic interaction of a pile with a transversely isotropic elastic half-space under transverse excitations. Int J Solid Struct 2014;51(23–24):4082–93.
[23] Amiri-Hezaveh A, Moghaddasi H, Karimi P, Ostoja-Starzewski M. Dynamic interaction of plates in an inhomogeneous transversely isotropic space weakened by a crack. ZAMM-Journal of Applied Mathematics and Mechanics/Zeitschrift für Angewandte Mathematik und Mechanik 2017;97(11):1338–57.
[24] Eskandari-Ghadi M, Amiri-Hezaveh A. Wave propagations in exponentially graded transversely isotropic half-space with potential function method. Mech Mater 2014;68:275–92.

[25] Karimi P, Amiri-Hezaveh A, Moghaddasi H, Sabet FA, Ostoja-Starzewski M. Elastodynamics of a multilayered transversely isotropic half-space due to the rigid motion of foundation. Wave Motion 2019;88:106–28.
[26] Ai ZY, Cao Z. Vibration isolation of row of piles embedded in transverse isotropic multi-layered soils. Comput Geotech 2018;99:115–29.
[27] Zhang S, Cui C, Yang G. Vertical dynamic impedance of pile groups partially embedded in multilayered, transversely isotropic, saturated soils. Soil Dynam Earthq Eng 2019;117:106–15.
[28] Ai ZY, Liu CL, Wang LJ, Wang LH. Vertical vibration of a partially embedded pile group in transversely isotropic soils. Comput Geotech 2016;80:107–14.
[29] Shahbodagh B, Ashari M, Khalili N. A hybrid element method for dynamics of piles and pile groups in transversely isotropic media. Comput Geotech 2017;85:249–61.
[30] Moghaddasi H, Shahbodagh B, Khalili N. Lateral vibration of piles and pile groups in nonhomogeneous transversely isotropic media. Int J GeoMech 2020;20(8):04020124.
[31] Poulos HG. Analysis of the settlement of pile groups. Geotechnique 1968;18(4):449–71.
[32] Kaynia AM. Dynamic stiffness and seismic response of pile groups. Doctoral dissertation, Massachusetts Institute of technology; 1982.
[33] Gazetas G, Fan K, Kaynia A, Kausel E. Dynamic interaction factors for floating pile groups. Journal of Geotechnical Engineering 1991;117(10):1531–48.
[34] Dobry R, Gazetas G. Simple method for dynamic stiffness and damping of floating pile groups. Geotechnique 1988;38(4):557–74.
[35] Mylonakis G, Gazetas G. Lateral vibration and internal forces of grouped piles in layered soil. J Geotech Geoenviron Eng 1999;125(1):16–25.
[36] Eskandari-Ghadi M. A complete solution of the wave equations for transversely isotropic media. J Elasticity 2005;81(1):1–19.
[37] Khojasteh A, Rahimian M, Eskandari M, Pak RYS. Asymmetric wave propagation in a transversely isotropic half-space in displacement potentials. Int J Eng Sci 2008;46(7):690–710.
[38] Peng Y, Sheng X, Lu J. Improvement to the fictitious pile method for pile-soil interaction problems. Soil Dynam Earthq Eng 2022;162:107465.
[39] Mitrinovic DS, Keckic JD. The Cauchy method of residues: theory and applications, vol. 9. Springer Science & Business Media; 1984.
[40] Ai ZY, Liu CL. Vertical vibration of a pile in transversely isotropic multilayered soils. J Sound Vib 2015;357:145–55.
[41] Kanellopoulos K, Gazetas G. Vertical static and dynamic pile-to-pile interaction in non-linear soil. Geotechnique 2020;70(5):432–47.
[42] Kagawa T. Dynamic lateral pile-group effects. Journal of Geotechnical Engineering 1983;109(10):1267–85.
[43] Gazetas G, Radhima J, Garini E. Inelastic stiffnesses of floating pile groups. In: Analysis of pile foundations subject to static and dynamic loading. CRC Press; 2021. p. 247–68.
[44] Graff KF. Wave motion in elastic solids. New York: Dover Publications; 1991.
[45] Shahbodagh B, Khalili N. Closed-form solutions for shear wave propagation and attenuation in multiphase porous media. Comput Geotech 2024;175:106660.
[46] Gazetas G. Analysis of machine foundation vibrations: state of the art. Int J Soil Dynam Earthq Eng 1983;2(1):2–42.
[47] Theland F, Lombaert G, François S, Pacoste C, Deckner F, Blom P, Battini JM. Dynamic response of driven end-bearing piles and a pile group in soft clay: an experimental validation study. Eng Struct 2022;267:114629.